Three-Phase Custom Power Active Transformer for Power Flow Control Applications

M. A. Elsaharty, *Member, IEEE,* J. Rocabert, *Member, IEEE,* J. I. Candela, *Member, IEEE* and Pedro Rodriguez, *Fellow, IEEE*

This paper presents the three-phase Custom Power Active Transformer (CPAT), characterized by the integration of power electronics in a transformer to facilitate grid services. Such integration enables step-up/step-down transformation between primary and secondary as well as shunt and series compensation services to the power system through a single transformer. The CPAT, can empower the grid with Flexible AC Transmission System (FACTS) and power quality services such as power flow control, reactive power compensation, active filter and voltage regulation through a single monolithic transformer. In this paper, designs of the three-phase CPAT are realized and analyzed based on their equivalent magnetic circuit as well as their structure requirements and constraints. Simulation analysis of the three-phase CPAT clarifies its capability to actively regulate power flow between the primary and secondary windings as well as achieve grid harmonic current compensation. Moreover, through real-time simulations and an experimental prototype, the merits and performance of the three-phase CPAT were further validated.

Index Terms

Power transformers, Magnetic circuits, Power control, Power Transmission

I. INTRODUCTION

The increase in peak customer demand of electrical energy, use of non-linear loads and increased line congestion, all have eventually affected power quality, system reliability, system stability and energy price [1]. In this regard, FACTS devices propose a high-performance and cost-effective solution for power system compensation demands. Such devices have proved to enhance and achieve better exploitation of transmission and distribution facilities [2]. In such compensation systems, the transformer is an essential element to adapt voltage levels between the power converter and electrical grid, as well as isolating both systems to avoid using complex power electronics structures [3]. Among the FACT devices, the Unified Power Flow Controller (UPFC) is the most versatile and powerful device in reduction of line congestion and increasing existing lines capacity [4]. However, typical

transformer-based connection of a UPFC and other high power compensation devices presented in literature have required special bulky transformers to achieve the required isolation, VA rating and desired voltage waveform [5]. Among the most effective approaches to resolve such issues, is the use of transformer-less UPFC [6-7] or power-electronics based transformers also known as the Smart Transformer [8-10]. A transformer-less UPFC configuration as well as the Smart Transformer, utilize a back-to-back converter configuration that provides robust dynamic control over power flow as well as auxiliary services to the grid using multilevel power-electronics topologies. Although such configurations have been commissioned and have successfully eliminated the requirement of bulky transformers [11-12], these configurations require complex power electronics structures and topologies, as well as power devices capable of supporting full load rated power/voltage [13].

Since the high-power transformers are an essential element in a power system to match the voltage level between different buses, it would be interesting to integrate in such a transformer series and shunt auxiliary connection to power electronics converters. Integration of both series and shunt transformers in a single power transformer would facilitate areas of the power system and the transformer itself with services in a single structure. Hence the structure would provide an isolated connection of fractional power converters to the system as well as reduce the footprint of the entire system, manufacturing cost and number of auxiliary equipment (tanks, bushings and protection), while providing the grid with series and shunt services.

The integration of shunt and series windings in a transformer structure, would isolate the grid and compensation system as well as provide power conditioning services to the grid using off-the-shelf converters. This has been proposed in several high-power topologies such as the integrated Static Synchronous Compensator (STATCOM) transformer [14], wound rotor induction machine based power flow control [15], magnetic amplifier based power flow control [16] and a series-shunt combining transformer [17]. The approaches presented in [14-16] have either proposed a single type of compensation integration or are limited to one specific application. The Sen Transformer (ST)proposed in [17] incorporates series and shunt compensation in a single transformer. The ST uses tap changers to inject a compensation voltage to operate as a UPFC with certain degrees of freedom [18]. However, the ST presents several limitations including use of tap changers which introduces limitations in the degrees of freedom as well as its inability to provide extra services to the grid such as power quality enhancement. Moreover, ST is not adequate for fast dynamic control over power flow since control is provided through step changes [19].

The CPAT presented in [20] and [21], demonstrates the possibility of incorporating power electronics in a single-phase transformer to provide shunt and series power quality services to the load and grid. However, for practical applications, compensation systems are implemented in three-phase [22]. In [20], the concept of expanding the CPAT to multi-phase systems has been presented but not yet analyzed or implemented.

This paper presents two three-phase CPAT configurations, one configuration uses three single-phase CPATs and another configuration uses a combined monolithic CPAT. The equivalent magnetic circuit of the proposed structures are presented and analyzed based on their operation constraints as well as manufacturing requirements compared to several three-phase compensation systems. Simulations of the proposed CPAT structures are evaluated for power flow control applications and elimination of transformer magnetizing current harmonics from the grid. Furthermore, experimental results on a stiff grid shows the capability of a CPAT to control power flow through its series winding as well as provide harmonics and reactive power compensation through its shunt winding.

This paper is organized as follows: Section II introduces the CPAT structures, model and theory of operation for power flow applications, Section III presents the benefits, constraints and the applicability of a three-phase CPAT in different compensation systems, Section IV shows the simulation evaluation of both proposed three-phase CPAT structures for power flow control application, Section V evaluates the performance of a three-phase CPAT through a real-time simulation on a 5-bus benchmark power system and an experimental prototype platform. Finally, conclusions are summarized in Section VI.

II. Theory of Operation of a three-phase CPAT

A. Configurations

The concept of the CPAT is based upon the magnetic circuits theory which states that windings wound on the same core limb are equivalent to parallel electrical circuits, while windings wound over shunt core limbs are equivalent to series electrical circuits [23]. Using this principle, Fig.1 shows a single-phase CPAT construction with voltages and currents represented in the form v_k, i_k where k represents the winding number (k=1,2,3,4) [20]. In this configuration, the primary (v_1) and secondary (v_4) voltages are coupled through the flux (Φ) traveling in the core limbs and yokes. Meanwhile, shunt current (i_2) and series voltage (v_3) provide the shunt and series compensation services as discussed in [21]. The three-phase converter in Fig.1 operates as two single-phase converters (converter legs ‘a’ and ‘b’) with a common leg ‘c’. Leg ‘a’ is connected to the series winding through an LC filter with the output voltage controlled to achieve the required series winding voltage. Leg ‘b’ is connected to the shunt winding

through an LCL filter with the output current controlled according to the required shunt winding current. The methodology presented in [24] is among the effective methods to control the common leg ‘c’ of the converter.

The configuration can be further extended to three-phase applications by using three single-phase CPATs with a three-phase four wire back-to-back converter configuration shown in Fig.2. Each connection type (primary, secondary, series and shunt) consists of one winding per transformer connected in Y configuration. In Fig.2, voltages and currents are represented in the form v_{pk}, i_{pk} where p represents phase number and k represents the winding number. The shunt and series variables are represented with k=2 and k=3, respectively. Both neutral wires (n_2, n_3) are connected to the common point of the DC bus.

To further integrate the configuration, the structure proposed in Fig.3 stacks the three CPATs on top of each other in a three-phase shell type monolithic structure. This integration of cores would share transformer yokes between each phase as well as reduce the setup footprint, tanks, bushings and protection equipment. Further clarification of the benefits of such configuration will be further clarified in Section III.

Both three-phase configurations consist of two three phase converters in back-to-back configuration. Conv.1 is connected to the shunt windings through an LCL filter to regulate the current injected in each shunt winding. In this study, Conv.1 is responsible of regulating the DC bus voltage, controlling reactive power through the primary winding as well as eliminate its harmonic current components. A split-capacitor topology has been utilized for the later to facilitate triplen harmonics injection in the shunt winding. Moreover, the shunt converter would regulate the DC bus voltage (v_{dc1} and v_{dc2}) to maintain system operation. Conv.2 is connected to the series windings through an LC filter to regulate the voltage injected in each phase winding. The operation of the series winding for power flow control applications is being considered in this study.

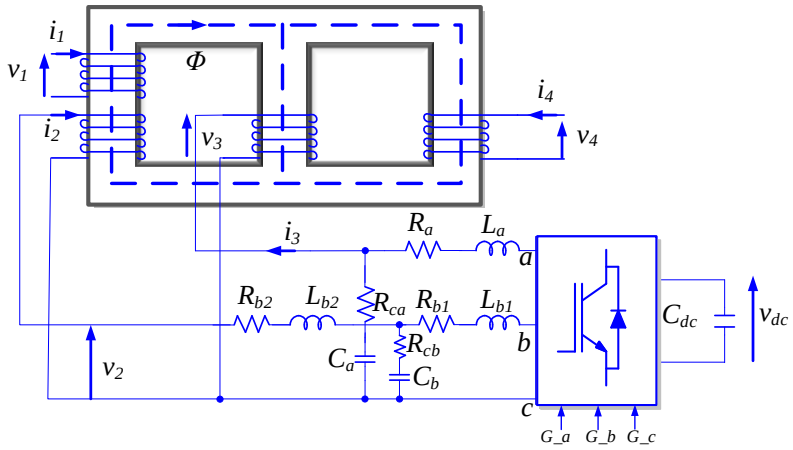

Fig. 1. Single-phase CPAT configuration.

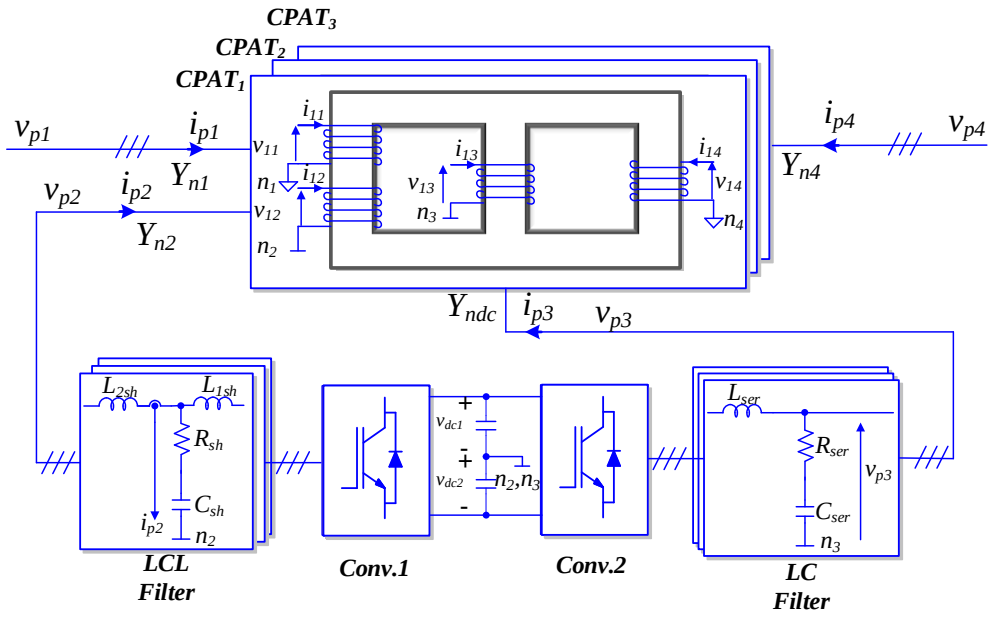

Fig. 2. Three-phase CPAT configuration.

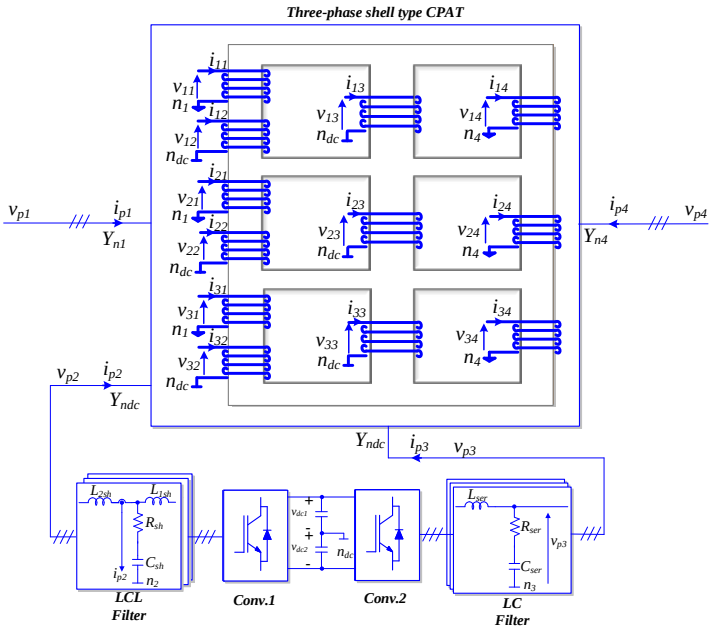

Fig. 3. Three-phase shell-type CPAT configuration.

B. MODELLING

1. SINGLE PHASE CPAT

Considering low frequency responses as the primary concern in FACTS applications, the conventional magnetic circuit based model is adopted to obtain a topologically correct equivalent model [21]. By discretizing the magnetic flux paths in the core of Fig.1, the equivalent model shown in Fig.4(a) can be deduced. Fig.4(a) consists *m* number of limbs and *k* winding types with *k*=1(primary), 2(shunt),3(series),4(secondary). Fluxes present in this circuit are characterized as core linkage fluxes (Φ_{cm}), winding fluxes (Φ_k), leakage fluxes per winding (Φ_{Lk}) and core leakage flux (Φ_0). Core limbs and yokes are represented by non-linear reluctances $\Re_Y$ and $\Re_L$ with a value calculated based on the B-H characteristics of the core material. A non-linear reluctance is modeled as a controlled magneto-motive source in a closed-loop between input flux and output magneto-motive force (*F*) as shown in Fig.4(b). This model would produce an opposing magneto-motive force based on the limb/yoke length (*l*), area (*A*) and the core B-H characteristics. Meanwhile, winding leakage reluctances ($\Re_k$) as well as core leakage reluctance ($\Re_0$) are represented by linear reluctances. Leakage reluctances are evaluated based on dimensions as in (1) using the flux path length, mean area and relative permeability of air($\mu_0=4\pi10^{-7}$). The flux generated by each winding is linked to a winding electric circuit shown in Fig.4(c) to model winding losses and core equivalent losses. For any applied winding voltage (v_k), the equivalent transformer winding currents (i_k) is dependent upon winding resistance (R_k), equivalent core loss resistance (R_c) and effective winding current (i_{ek}). The effective current is calculated based on the effective magneto-motive force (F_k) of the winding and number of turns (N_k) as shown in Fig.4(c). Whereas, the winding flux in the magnetic circuit is deduced from the effective voltage (v_{ek}) in the winding electric circuit.

$$\Re_0, \Re_k = \frac{l}{4\pi 10^{-7} A} \quad (1)$$

It is worth to be noted that to overcome algebraic loops due to the coupling between electric, magnetic and non-linear reluctance circuit, a one-simulation-step-time delay is applied. However, such an approach should be considered with high sampling-rate to avoid numerical oscillations.

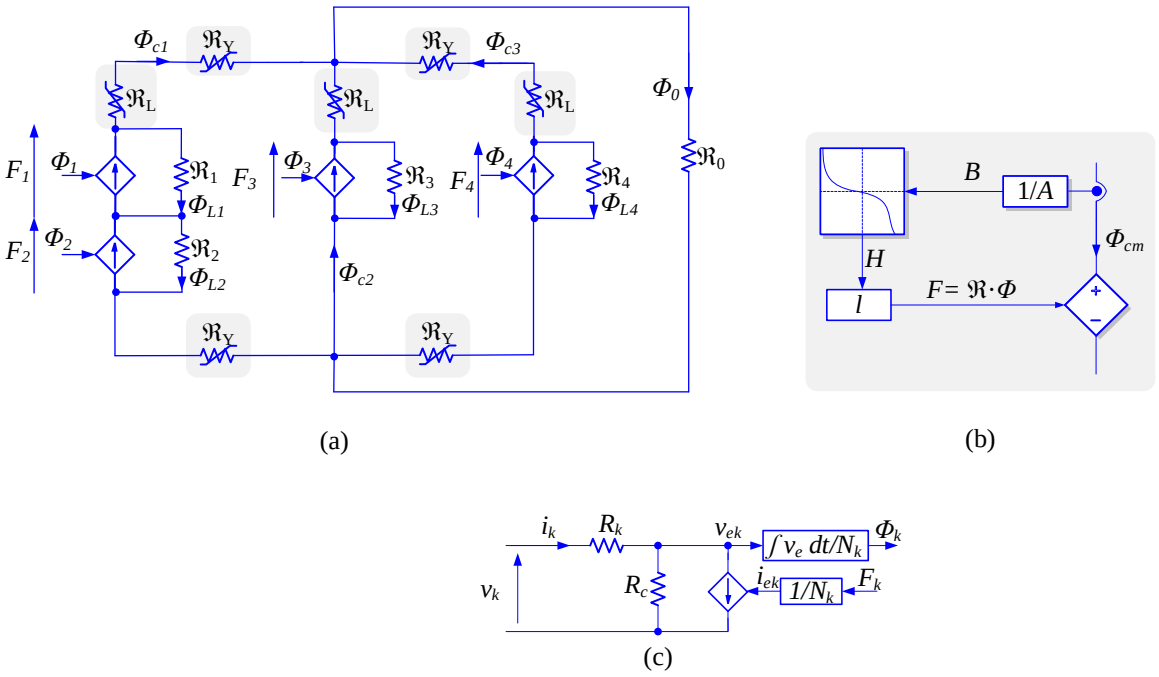

Fig. 4. Magnetic circuit model of a single-phase CPAT. (a) Core magnetic circuit, (b) non-linear reluctance model and (c) winding electric circuit model.

Using duality transformation [25], the equivalent electric circuit shown in Fig.5 can be deduced from Fig.4. The equivalent non-linear core parameters (R_{en}, L_{en}) are modeled in series rather than in parallel to reduce the number of loop currents and simplify the derivation of equivalent state-space model. The primary and secondary limbs core parameters (R_{e1}, L_{e1} and R_{e3}, L_{e3}) are equivalent to one limb and two yoke impedances whereas the series limb parameters (R_{e2}, L_{e2}) is equivalent to one limb impedance. It can be preliminary observed that the equivalent electric circuit shown in Fig.5 consists of a parallel branch to the primary and a series branch between the primary and secondary. It should be noted that core impedances are typically large due to the low equivalent core reluctance of each core limb and yoke. Meanwhile, leakage impedances are significantly lower than core impedances. Therefore, in an ideal transformer scenario, the primary, shunt, series and secondary windings are perfectly coupled.

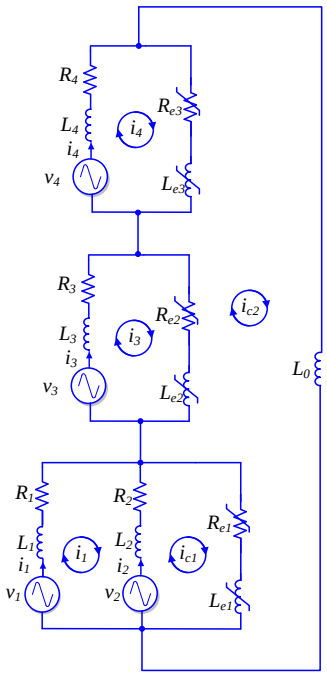

Fig. 5. Equivalent electric circuit of a single-phase CPAT.

2. THREE-PHASE SHELL TYPE CPAT

In a three-phase system consisting of three single-phase CPATs as in Fig.2, the CPATs are not coupled magnetically to one another and the equivalent model would be a repetition of the single-phase model shown in Fig.4. The three-phase shell-type CPAT shown in Fig.3, stacks three single-phase CPATs on top of each other such that each phase shares a common yoke with another phase. The equivalent magnetic circuit shown in Fig.6 is represented by fluxes (Φ_{pk}, Φ_{Lpk}, Φ_{Ypm}, Φ_{cpm}), magnetomotive forces (F_{pk}), linear reluctances ($\Re_{pk}$, $\Re_{0}$) and non-linear reluctances ($\Re_{Y1}$, $\Re_{Y2}$) such that p is the phase number, k is the winding number and m is the limb/yoke number. It should be noted that according to this design, the common yokes ($\Re_{Y2}$) are initially assumed double the size of the outer yokes ($\Re_{Y1}$) such that the core structure is equal to three single-phase CPATs. Core flux paths are divided into common yoke fluxes (Φ_{Ypm}) and limb fluxes (Φ_{cpm}). The effect of the shared yokes can be realized in the equivalent electric circuit shown in Fig. 7 where the shared yoke impedance can be observed between phase 1,2 (R_{Y1}, L_{Y1}, R_{Y2}, L_{Y2}) and between 2,3 (R_{Y3}, L_{Y3}, R_{Y4}, L_{Y4}). Each of the equivalent parameters R_{e11}, L_{e11}, R_{e13}, L_{e13}, R_{e31}, L_{e31}, R_{e33} and L_{e33} represent one limb and yoke. The parameters R_{e12}, L_{e12}, R_{e22}, L_{e22}, R_{e32}, L_{e32}, R_{e21}, L_{e21}, R_{e23} and L_{e23} each represent one limb.

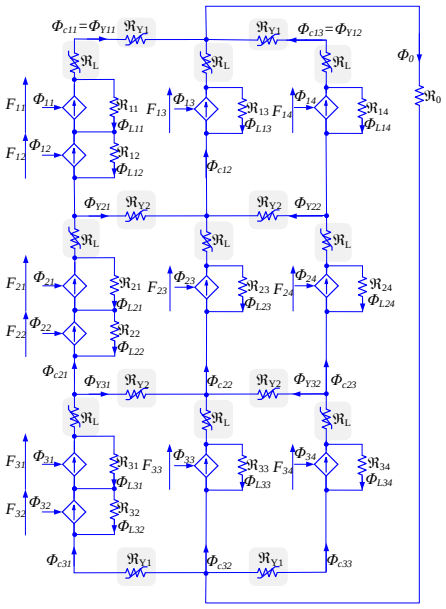

Fig. 6. Equivalent magnetic circuit of a three-phase shell type CPAT.

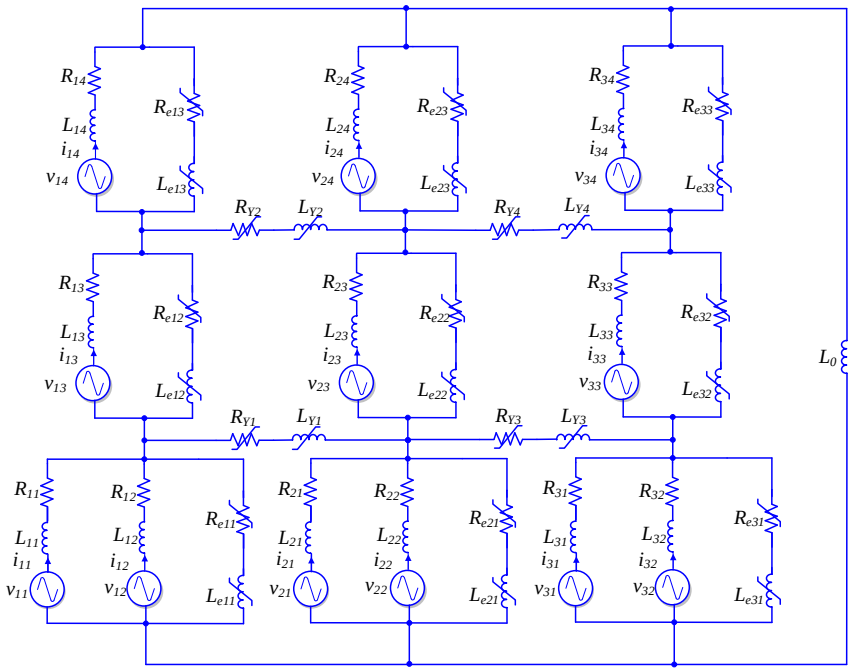

Fig. 7. Equivalent electric circuit of a three-phase shell type CPAT.

Due to the complexity of the circuit shown in Fig.6 and Fig.7, only the magnetic-circuit model is taken into consideration in this paper since the circuit consists of 26 states which is too complex to realize. Therefore, analysis based on the applicability and operation capability of this transformer is taken into consideration in this paper. In depth analysis of different operation states, transients and design considerations are to be investigated in forthcoming research.

C. OPERATION

By analyzing a single-phase CPAT in power flow applications, the other phases can be considered a repetition. In this analysis, it is assumed that the single-phase CPAT shown in Fig.4(a) is connected to a stiff grid on primary and secondary windings, i.e. v_1 and v_4 are constant. Hence, neglecting the effect of winding and core loss resistance, Φ_1 and Φ_4 would be constant as well. Meanwhile, F_1, F_2 and F_4 are variable depending on the current in their respective winding. With a fixed flux through the core between the primary and secondary, the flux Φ_3 would be responsible of changing the magneto-motive force of the central limb which results in a change in the primary and secondary magneto-motive forces. The following analysis would further clarify this state of operation of a CPAT.

Using Gauss's law and Ampere's law, the relationship in (9) can be derived based on the equivalent magnetic circuit in Fig.4(a). Based on (9), the effective current in the secondary winding (i_{e4}) is coupled to the flux in the primary(Φ_1), secondary (Φ_4) and series (Φ_3) windings as well as the magneto-motive force in the primary (F_1) and series (F_3) windings. Assuming an ideal transformer, the effect of core reluctances can be considered minimal based on the core material used and as long as the flux through the core is in the linear operation region of the B-H characteristics [20]. Therefore, neglecting the effect of core reluctances, the magnetomotive forces would be equal such that $F_1 + F_2 \approx F_3 \approx F_4$. Using this assumption, the current in the secondary winding (i_4) would be dependent on Φ_1, Φ_2, Φ_3 and F_2 as shown in (10). Considering that Φ_1 and Φ_4 are constants, i_4 would be affected by Φ_3 and F_2 which are equivalent to series winding voltage (v_3) and shunt winding current (i_2). It can be concluded that the required v_3 to regulate i_4 is dependent mainly on the leakage reluctances.

$$F_4 = N_4 i_{e4} = \frac{\Re_4(\Phi_4(2\Re_Y\Re_0\Re_1\Re_3 + \Re_L\Re_0\Re_1\Re_3 + \Re_1\Re_3) + \Phi_1\Re_1\Re_3 - F_1\Re_3 + \Phi_3\Re_1\Re_3 - F_3\Re_1)}{\Re_1\Re_3(2\Re_Y\Re_0 + \Re_L\Re_0 + \Re_0\Re_4 + 1)} \quad (9)$$

$$F_4 \approx N_4 i_4 \approx \frac{\Phi_4 + \Phi_1 + \Phi_3 + \frac{F_2}{\Re_1}}{\Re_0 + \frac{1}{\Re_1} + \frac{1}{\Re_3} + \frac{1}{\Re_4}} \quad (10)$$

Similarly, the magnetomotive force in the primary winding (F_1) can be represented as in (11). Using the previous assumption of neglecting core reluctances, the equation results in the ideal transformer state where $F_1 + F_2 \approx F_4$. This entails that the current in the primary winding (i_1) is dependent on the current supplied through the shunt winding (i_2) as well as the current in the secondary winding (i_4). Therefore, the shunt winding can provide harmonic and fundamental current components eliminating their requirement from the primary winding.

$$F_1 = N_1 i_{e1} = \frac{(2\Re_Y + \Re_L)\Re_1\Re_4(\Phi_1 - \Phi_4) - F_2\Re_1\Re_4 + F_4\left(\Re_1\Re_4 - \Re_1(2\Re_Y + \Re_L)\right)}{\Re_1\Re_4 + \Re_4(2\Re_Y + \Re_L)} \quad (11)$$

III. Design Considerations

A. Windings

Certain design aspects must be taken into consideration for selection of appropriate shunt and series converters of a CPAT. As discussed in [20] and [21], the CPAT reduces the total number of windings required to implement a series-shunt compensation system. The preliminary design ratio values of the primary and secondary turns (N_1, N_4) are determined as in a typical transformer through their required operating voltages in (12). With a pre-determined shunt converter voltage, the shunt winding turns (N_2) can be estimated using (12). Moreover, the relationship in (13) should be maintained in the determining the maximum primary, shunt, series and secondary winding current (i_{1max}, i_{2max}, i_{3max}, i_{4max}). With a pre-determined series converter current, the series winding turns (N_3) can be estimated using (13).

$$\frac{v_1}{N_1} = \frac{v_4}{N_4} = \frac{v_2}{N_2} \quad (12)$$

$$N_1 i_{1max} + N_2 i_{2max} = N_3 i_{3max} = N_4 i_{4max} \quad (13)$$

In a CPAT, the series voltage varies depending upon design parameters as well as voltage and current across each winding. Using pre-determined design parameters, the equivalent magnetic circuit in Fig.4 can be utilized to determine the resultant series voltage under various operating points for a selected number of turns. Neglecting the effect of core-reluctances and leakage reluctances, the maximum open-circuit voltage across the series winding can be expressed as follows:

$$v_{3max} = N_3\left(\frac{v_1}{N_1} + \frac{v_4}{N_4}\right) = 2v_1\frac{N_3}{N_1} \quad (14)$$

B. Structure

A three-phase CPAT can be compared in structure to a three-phase series-shunt compensation system consisting of single-phase shell type transformers and three-phase core type transformers. Using the methodology discussed in [20] to determine the core size reduction, three compensation scenarios are compared to a three-phase CPAT. The results of this comparison are tabulated in the following subsection.

The first configuration compares a three-phase CPAT to a three-phase compensation system consisting of three single-phase shell type shunt transformers, series transformers and power transformers such that the power

transformer is between both compensation transformers as shown in Fig. 8. Each transformer consists of limbs type a_1, c_1 and yokes b_1. As in the methodology presented in [20], it is assumed that limbs type a_1 and yokes type b_1 are equal, while limb type c_1 is considered double the size of type a_1 due to its required power handling capability. Moreover, it is assumed that the relationship between the core size of each power transformer and each compensation transformer is linear for all core elements.

The structure of a three-phase shell type CPAT can be divided similarly into core limbs and yokes as shown in Fig.9. In a CPAT, limbs a_2 and yokes b_2 are considered to be equal and double the size of a typical single-phase shell type transformer ($a_2 = 2a_1$) due to their required power handling capability. Series compensation limbs are of the same core size as a typical compensation transformer with a core size reduction factor m_1. Design of the common yokes between phases is based on the core material capability to operate without saturation. The common core factor m_2 would have a value between 1 to 2, which is equivalent to three single-phase CPATs stacked on top of each other (m_2=2) and three single-phase CPATs sharing one yoke of the same size as all other yokes (m_2=1).

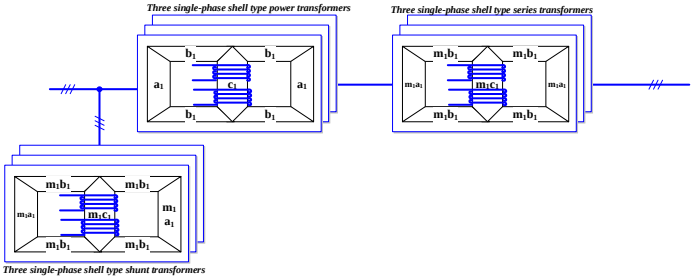

Fig. 8. Configuration of a three-phase compensation system using single-phase transformers

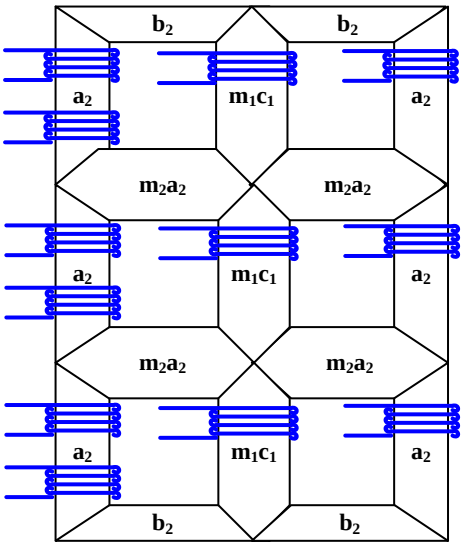

Fig. 9. Core limbs and yokes elements of a three-phase shell type CPAT

In the second configuration, a three-phase CPAT is compared to a three-phase compensation system consisting of a three-phase shunt transformer, three-phase series transformer and three-single phase shell type power transformers such that the power transformer is between both compensation transformers as shown in Fig. 10. Since windings in a three-phase transformer are wound on each limb, it is assumed that each limb in a compensation transformer to be a factor of the power handling limb c_1.

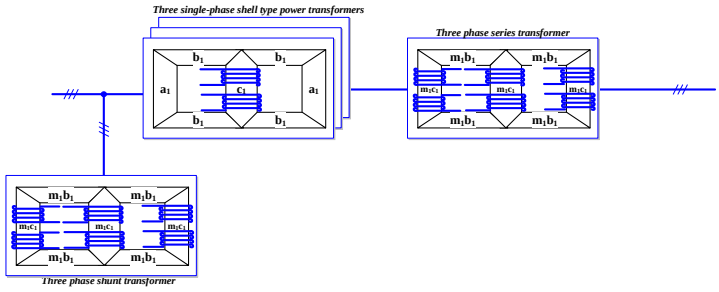

Fig. 10. Configuration of a three-phase compensation system using single-phase power transformers and three-phase compensation transformers

The last configuration compares a three-phase CPAT with three three-phase transformers as in Fig.11. Notice that each limb in the power transformer has been labeled c_1 since all limbs are equal and handle power delivery between primary and secondary.

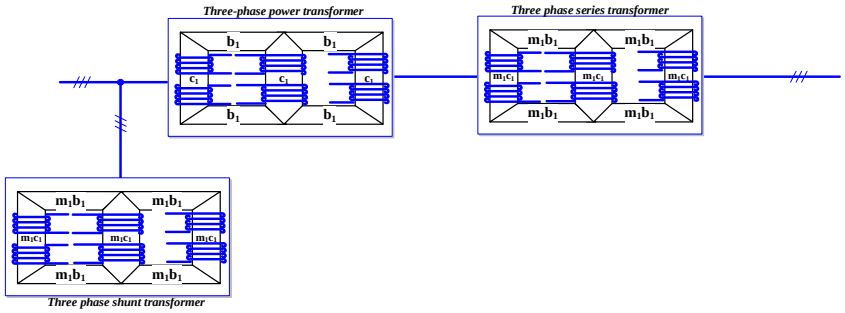

Fig. 11. Configuration of a three-phase compensation system using three-phase transformers.

C. SUMMARY

Table I shows the comparison summary of a three-phase CPAT in terms of reduction in number of windings, number of tanks and core size. It can be observed a CPAT would reduce the number of windings required as compared to any other configuration. In terms of number of tanks, the CPAT in Fig.2 requires the same number tanks as compared to the typical three-phase compensation system shown in Fig.11. However, the three-phase shell type CPAT in Fig.3 is beneficial in this case due to its monolithic structure. Core-size of a three-phase CPAT as

compared to Fig.11 is not beneficial mainly due to the larger core yokes required for better coupling between primary and secondary limbs. However, if a CPAT is compared to the systems in Fig.8 and Fig.10, core size reduction is possible under the constraints of m_1 and m_2.

Table I

Evaluation of CPAT vs. other transformer configurations

	CPAT configuration	Compensation configuration		
		Fig. 8	Fig. 10	Fig. 11
Number of windings reduction	Fig. 3	Yes (33.3%)		
	Fig. 2			
Number of tanks reduction	Fig. 3	Yes (88.8%)	Yes (80%)	Yes (66%)
	Fig. 2	Yes (66.6%)	Yes (40%)	Equal
Core Size reduction	Fig. 3 (m_2=1)	Yes (m_1>9.5%)	Yes (m_1>28.6%)	No (m_1>128.5%)
	Fig. 2	Yes (m_1>28.6%)	Yes (m_1>85%)	No (m_1>185.7%)

The proposed three-phase shell type CPAT is similar in shape to a typical three-phase shell type transformer. However, a three-phase shell type transformer has the power handling limbs in the center of the transformer, while the outer limbs handle the core energizing flux and the zero-sequence component arising from unbalance. Meanwhile, a three-phase shell type CPAT has significantly larger outer limbs for handling the power exchange and smaller central limbs to handle the series compensation power. Common yokes as well are significantly larger in the proposed structure since the flux flowing through such yokes is produced mainly by the power handling windings. Though, the proposed structure can be considered as a modified three-phase shell type transformer. Such structure provides the required voltage transformation between the primary and secondary as well as providing grid services through isolated connection of fractional power converters.

IV. Simulation Analysis

Based on the analysis in Section II, the three-phase CPAT can be used to regulate power flow between the primary and secondary winding as well as regulate harmonics and reactive power in the primary winding. The configuration in Fig.2 will be analyzed with a control setup to achieve these demands. To realize the limitations of a

CPAT to operate as a UPFC, Fig.3 has been analyzed with a series voltage sweep test up to the rated transformer voltage.

Using the modelling approach discussed in Section II, the CPAT configurations in Fig.2 and Fig.3 have been modeled based on the parameters presented in Table II. The transformer model consists of number of turns *N*, limb length l_L, yoke length l_Y and limb area *A*. Common core yokes between phases in Fig.3 were considered double the area of other yokes (m_2=2) and all core material follow a flux density (*B*), flux intensity (*H*) relationship shown in Fig.12.

In this analysis, primary and secondary windings were connected to the same source grid such that the CPAT would inject a voltage between these windings to control the power flow. This entails that at nominal operation while both shunt and series converters disabled, there would be no power flow between the primary and secondary since they are both excited with an equal voltage.

TABLE II

CPAT and Converter Parameters

Parameter	Value
Grid voltage/phase	220V
v_{p1}, v_{p2}, $v_{p3,}$ v_{p4}	240V, 240V, 480V,240V
i_{p1}, i_{p2}, i_{p3}, i_{p4}	70A, 7.2A, 7.2A, 70A
R_{pk}, R_c	0.02 p.u., 0.02p.u.
l_L, l_Y	0.51m, 0.3m
A	0.0156 m^2
N_{p1}, N_{p2}, N_{p3}, N_{p4}	50, 50, 100, 50
V_{dc}	700V
9Sampling Frequency, Switching Frequency	10kHz
C_{dc}	20mF
L_{1sh}, L_{2sh}, L_{ser}	6mH, 2mH, 7mH
R_{sh}, R_{ser}	4.7Ω, 2.35 Ω
C_{sh}, C_{ser}	5µF, 10µF

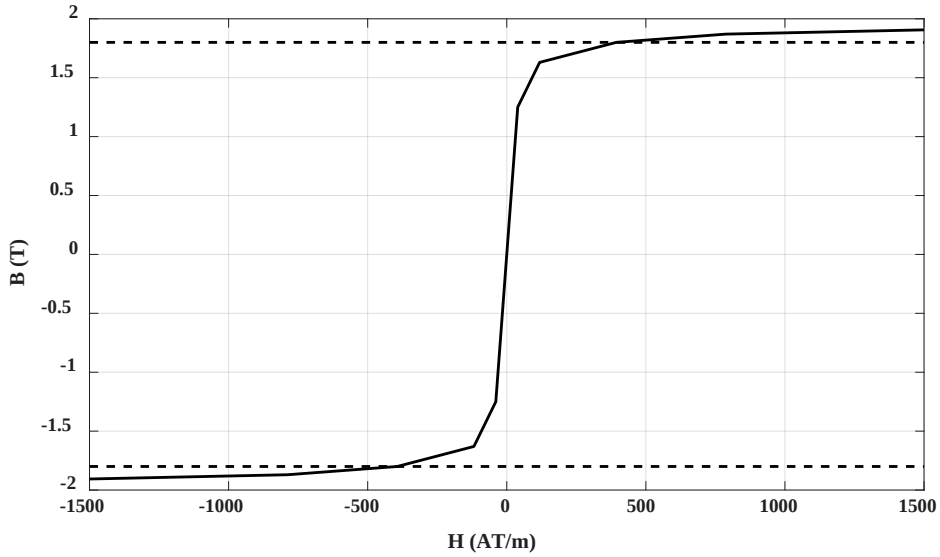

Fig. 12. BH characteristics of the core material with 1.8T nominal flux density.

In this setup, each converter operates independently with no link between the shunt and series converter except the measured grid voltage. The shunt converter has three functions which are to maintain a constant DC bus voltage, control reactive power through the primary and eliminate harmonic currents present at the primary winding. Meanwhile, the series converter controls the active and reactive power through the secondary winding according to a set reference.

A. SHUNT CONTROLLER

The utilized Shunt Controller shown in Fig.13 consists of DC Bus controller, Reactive Power Controller, Harmonics Controller and a Shunt Current Controller. The DC Bus controller maintains a constant DC bus voltage across both DC capacitors using two PI controllers which generates the reference direct and zero sequence components of the shunt converter current (I_{2d}^*, I_{20}^*). These components achieve split capacitor voltage balance (v_{dc1}, v_{dc2}) as well as a total DC bus voltage (v_{dc}) control to match the reference DC bus voltage (V_{dc}^*).

The Reactive Power Controller generates the quadrature component of the reference shunt converter current (I_{2q}^*) through a PI controller. The reference primary reactive power (Q_1^*) is set by the user and the controller achieves the required primary reactive power (Q_1) which is calculated using (15).

$$Q_1 = \frac{1}{\sqrt{3}}[v_{11} \quad v_{21} \quad v_{31}]\begin{bmatrix} 0 & -1 & 1 \\ 1 & 0 & -1 \\ -1 & 1 & 0 \end{bmatrix}\begin{bmatrix} i_{11} \\ i_{21} \\ i_{31} \end{bmatrix} \quad (15)$$

The *dq0* components of the reference shunt converter current are transformed to their equivalent three-phase reference fundamental component (i_{p2f}^*) through the primary synchronizing signal (θ_1). A Double Second-Order Generalized Integrator Frequency Locked Loop (DSOGI-FLL) [20] is utilized in each converter controller to determine the synchronizing signals (θ_1, θ_4) and frequencies (ω_1, ω_4). However, both signals are equal since as mentioned earlier that both the primary and secondary are excited by the same voltage.

The Harmonics Controller consists of several cascaded Resonant Controllers tuned to the required harmonics attenuation frequencies such that the resulting reference shunt harmonic currents (i_{p2h}^*) would attenuate the primary current harmonics. Finally, the Shunt Current Controller determines the reference output voltage of the shunt converter (v_{p2}^*) through a Proportional Resonant (PR) controller tuned to the primary fundamental frequency (ω_1).

It should be noted that the CPAT in [20] consisted of a Reactive Power Compensator in series to the DC Bus Controller which acted on controlling the primary current through the shunt winding. It is possible to implement such control configuration in this setup as well to investigate inrush current mitigation through the CPAT. However, this topic is outside the scope of this paper.

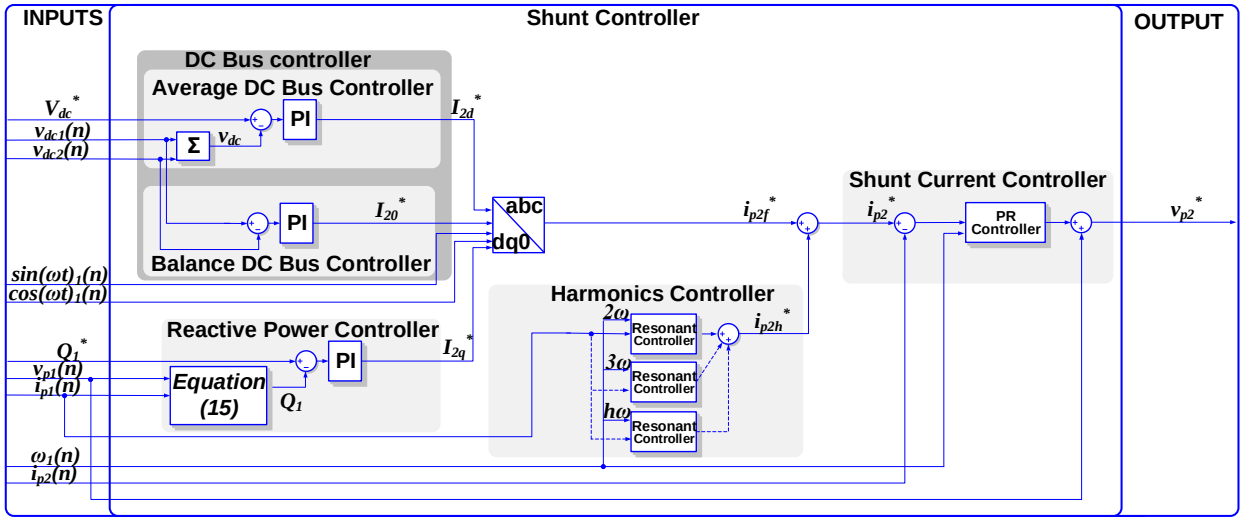

Fig. 13. Shunt converter controller structure.

B. Series Controller

The Series Controller discussed in [26] is shown in Fig.14 consisting of two control loops. The PQ Controller generates the reference stationary reference frame of the secondary current ($i_{4\alpha}^*$, $i_{4\beta}^*$) using reference active power (P_4^*), reactive power (Q_4^*) and stationary reference frame secondary voltage values ($i_{4\alpha}^*$, $i_{4\beta}^*$) as in (16). The components $i_{4\alpha}^*$ and $i_{4\beta}^*$ are transformed to their equivalent three-phase quantities (i_{p4}^*) for the reference of the

Secondary Current Controller which uses a PR controller tuned to $\square_4$ to generate the reference output series voltage (v_{p3}^*).

$$[i_{\alpha 4} \quad i_{\beta 4}] = \frac{1}{{v_{\alpha 4}}^2 + {v_{\beta 4}}^2} [{P_4}^* \quad {Q_4}^*] \begin{bmatrix} v_{\alpha 4} & -v_{\beta 4} \\ v_{\beta 4} & v_{\alpha 4} \end{bmatrix} \quad (16)$$

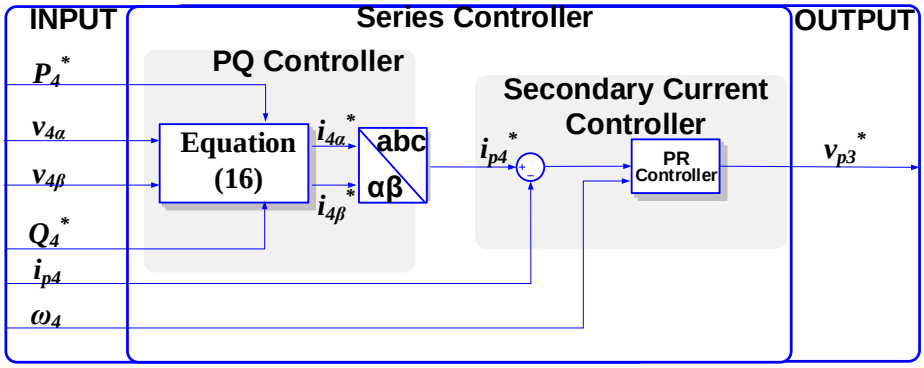

Fig. 14. Series converter controller structure.

C. SIMULATION RESULTS OF THREE PHASE CPAT

With the primary and secondary windings excited, the primary current shown in Fig.15(a) illustrates the waveform of the CPAT magnetizing current and DC bus charging current. Fig.15(a) shows that the primary current consists of 2nd, 3rd and 5th order harmonics at 5%, 20% and 10% of the fundamental frequency magnitude. The Harmonics Controller, tuned to these harmonic components, has reduced each component to less than 5% of the fundamental frequency as shown in Fig. 15(b). On the secondary side of the CPAT, the secondary current remains supplying the harmonic currents required to magnetize this side of the CPAT. Elimination of such harmonic currents is possible through a shunt winding at the secondary limb as in the generalized configuration shown in [20]. In such a configuration, the required magnetizing current by the CPAT would be supplied through two shunt converters. This paper focuses on the concept of supplying magnetizing currents through the shunt winding of a CPAT while total magnetization through several converters is outside the scope of this paper.

The reference primary reactive power was set to 0kVAR such that all the reactive power required by the transformer will be supplied through the shunt converter. At the instant shown in Fig.16, the Reactive Power Controller was enabled which increased Q_2 from the shunt converter to match the required power by the transformer. Notice the change in Q_1 from 500VA to 0VA as the Reactive Power Controller was enabled as the shunt converter injects the required reactive power Q_2. Meanwhile, the shunt converter absorbs active power P_2 to maintain a constant DC bus voltage.

Power flow control was achieved as shown in Fig. 17 by enabling the Series Controller with a reference active and reactive power of 8kW and 2.5kVAR, respectively. The Series Controller injects reactive power Q_3 through the series winding hence changing the power flow according to the required reference P_4 and Q_4. Active Power supplied through the series converter P_3 is mainly to compensate for winding resistance losses and core losses.

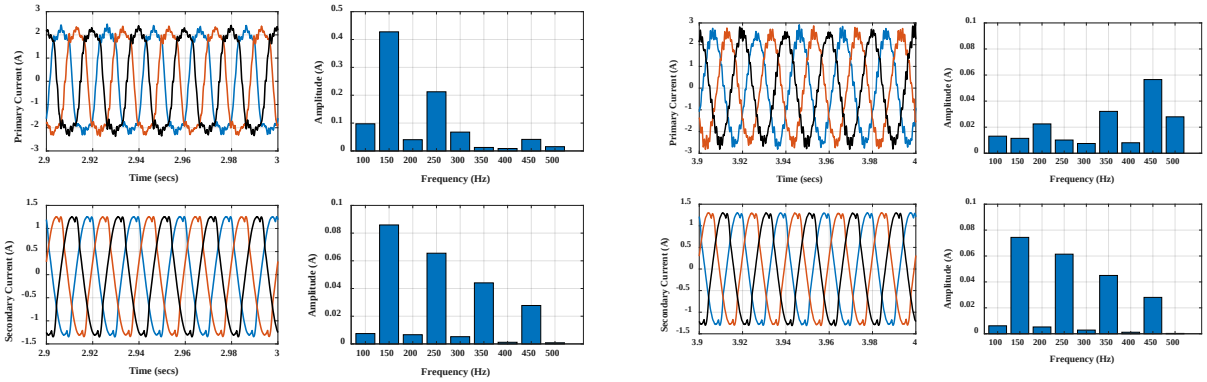

(a) (b)

Fig.15. Primary current waveform and harmonics (a) without harmonic compensation and (b) with harmonic compensation.

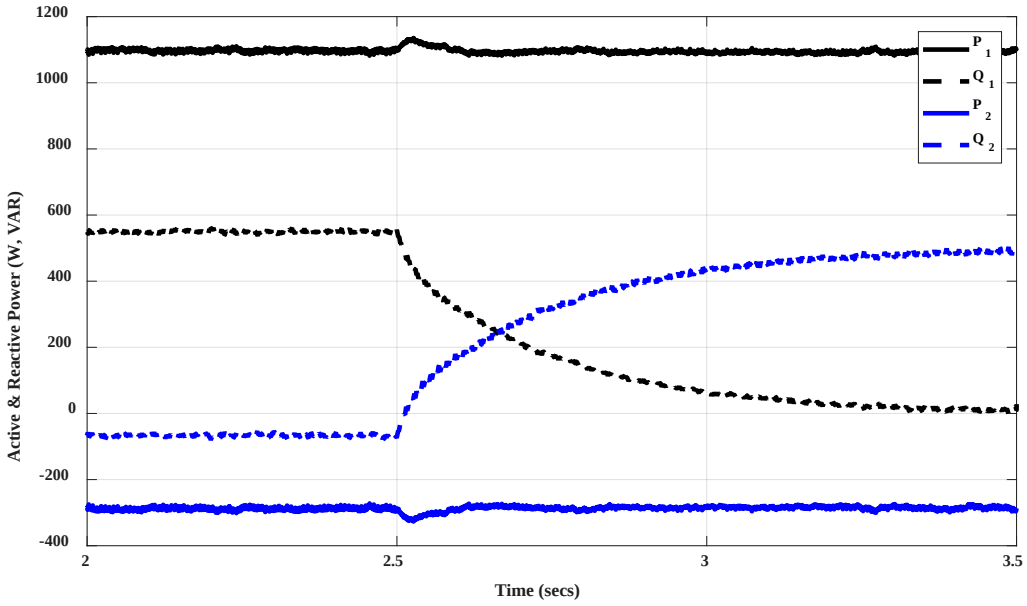

Fig. 16 PQ of primary and shunt winding during activation of Reactive Power Controller.

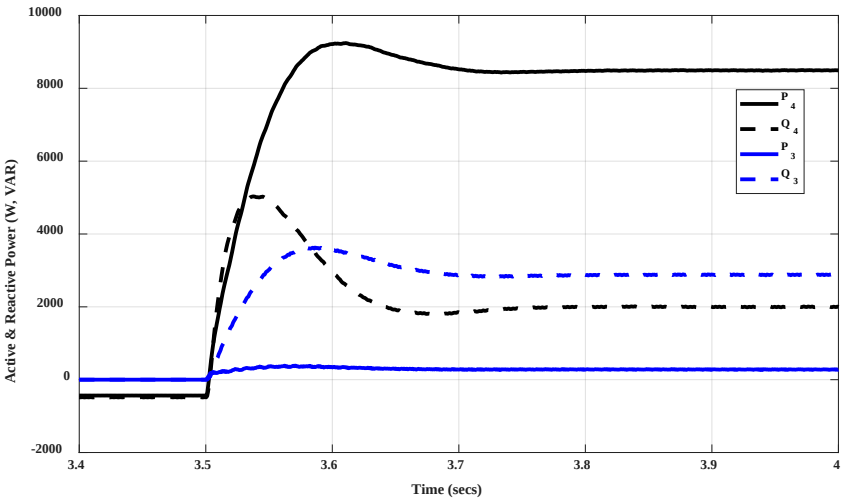

Fig. 17. PQ of secondary and series during activation of Series Controller.

D. SIMULATION RESULTS OF THREE-PHASE SHELL TYPE CPAT

With a common voltage at the primary and secondary windings of the CPAT in Fig.3, a magnitude and angle sweep test was performed on the series winding with a maximum voltage of 480V/phase. The result illustrated in Fig.18 shows the ability of the CPAT to control the active and reactive power flow between primary and secondary according to the applied series voltage. Under such test condition, the series winding supplies reactive power to vary the impedance between the primary and secondary hence varying the power flow between them. The contour shown in Fig.18, illustrates the maximum permissible power flow control that can be maintained with the selected series converter in Table II. Based on the utilized model and converter, 23% of the maximum power can be controlled using the selected series converter. The relationship between the maximum power flow control that can be achieved with the utilized CPAT and series converter power is shown in Fig. 19.

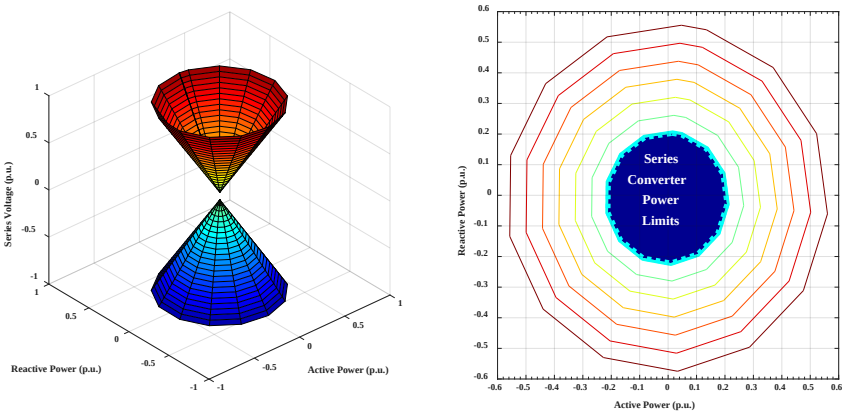

Fig. 18. Sweep test of three-phase shell type CPAT and its equivalent contour showing operation limits.

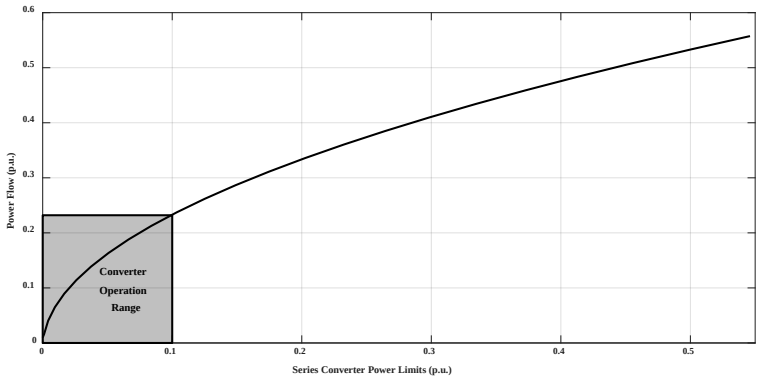

Fig. 19. Relationship between series converter power limit and maximum power flow.

To investigate the effect of the common limb in a three-phase shell type CPAT, the common yokes are assumed to be 1.3 times the size of other yokes (m_2=1.3). A comparison in harmonic contents between three single-phase CPATs and three-phase shell type CPAT is shown in Fig.20. The results show the similarity in both configurations results as well as the effectiveness of the shunt converter to eliminate the tuned harmonic components.

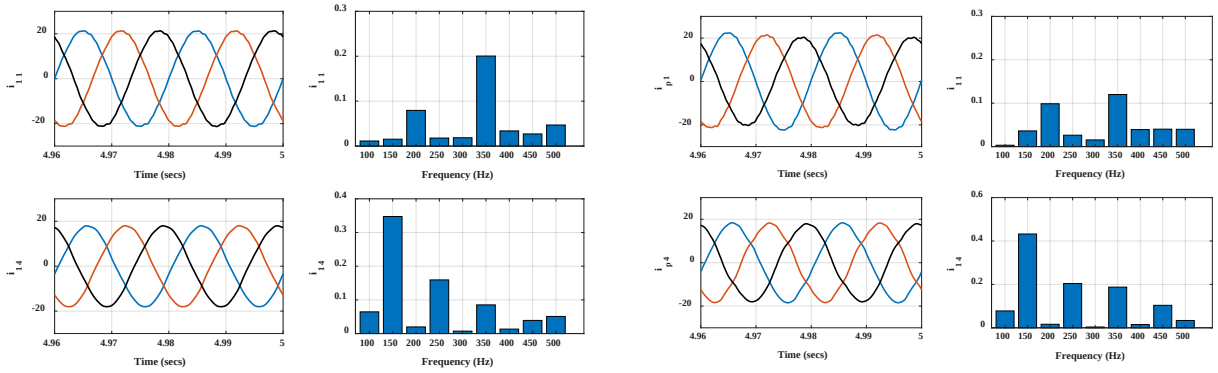

(a) (b)

Fig. 20. Harmonic spectrum of primary and secondary current with compensation. (a) Three-single phase CPATs and (b) Three-phase shell type CPAT.

E. HYSTERESIS AND SATURATION EFFECT

As discussed in [20] and [21], the hysteresis effect of the core mainly affects the primary and secondary current harmonics. For the three-phase CPAT results in Fig.16 and Fig.17, the limb fluxes shown in Fig. 21 presents the operation BH characteristics of the core limbs with respect to the core characteristics. It can be observed that the primary and secondary limbs operate at the nominal range shown in Fig. 12. However, the central limb operates at a lower range since the required injected voltage is much lower than the rated voltage of the central winding. Similarly, this can be observed in the three-phase shell-type CPAT limbs and yokes in Fig. 22 for the results

presented in Fig.20. Since the common yokes has been selected to be twice the size of outer yokes, it can be seen that the common yoke size can be further reduced in size to further utilize the core.

Assuming a 10% increase in the injected primary and secondary voltage, the core flux would operate outside the design boundaries of the BH characteristics and saturation of the core during each cycle is eminent. In such a case, low order harmonics would significantly increase at the primary and secondary side as shown in Fig. 23. Thanks to the shunt harmonics controller, it can be observed that the primary current low order harmonics do not increase as much as the secondary since the shunt controller provides such harmonic saturation currents to the primary side of the transformer.

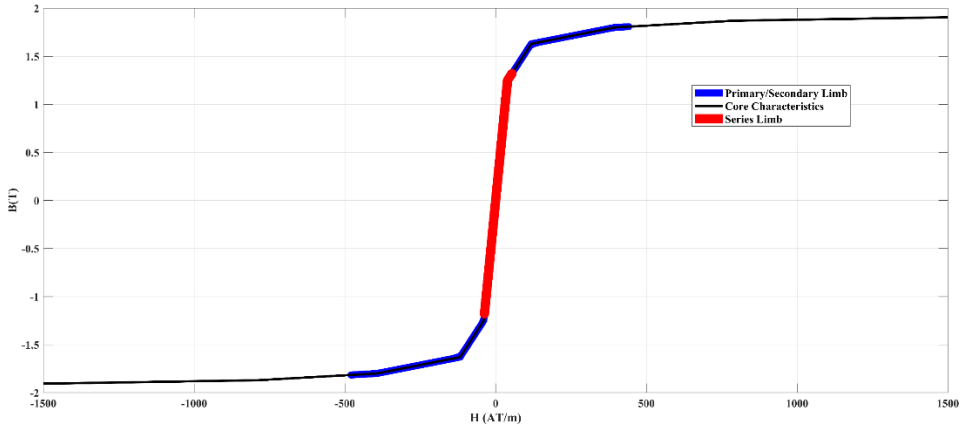

Fig. 21. BH characteristics of core limbs in a three-phase CPAT during nominal operation.

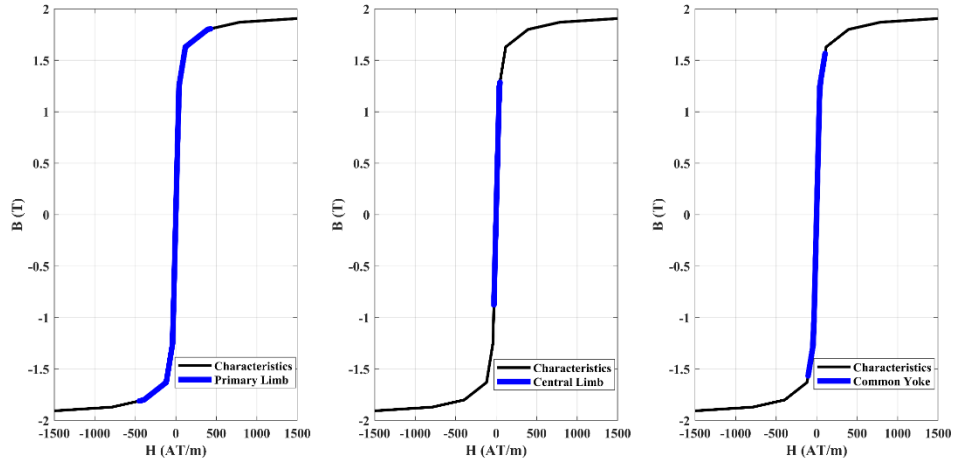

Fig. 22. BH characteristics of core limbs and common yoke in a three-phase shell-type CPAT during nominal operation.

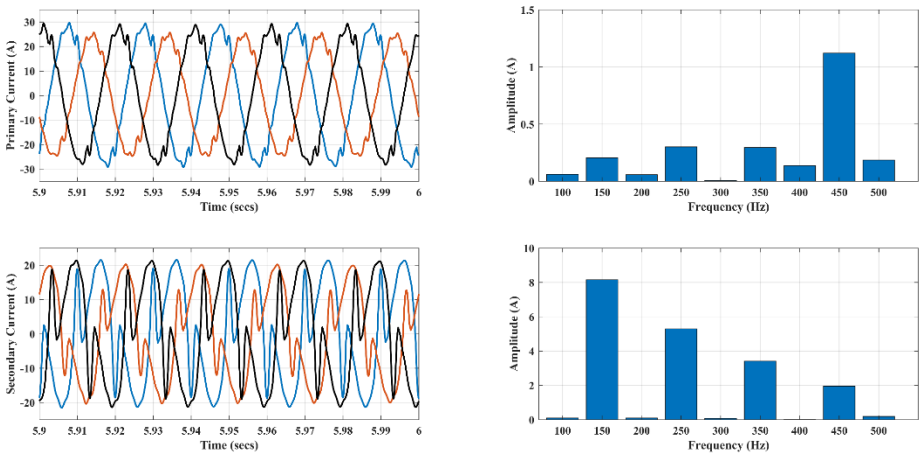

Fig. 23. Primary and secondary current under core saturation due to overvoltage.

V. Experimental Results

A. Stiff Grid

The configuration in Fig.2 was implemented as shown in Fig.21 using three 50kW, three-phase multi-winding transformers, each representing a single-phase CPAT with the parameters presented in Table II. Each phase of the transformer consists of 240V/240V/2.1kV windings each rated at 69.5A/7.2A/7.2A. Primary and secondary windings are considered to be the windings on the left and right limb, respectively (phase 'a' and phase 'c' of the three-phase transformer). Two 5kW converters controlled via two DS1103 were utilized for shunt and series compensation.

In this transformer, there are three set of windings available at the center limb. The 240V/69.5V and 240V/7.2A windings were connected in series to achieve higher voltage ratings and lower current requirement. The left limb and right limb 240V/69.5A windings are connected to a common stiff grid of 220V. The shunt converter is connected to the 240V/7.2A winding of the left limb to preform shunt compensation. A DC power supply was used to start-up the setup, then the power supply was switched off while the shunt converter regulated the DC Bus to a constant 700V.

Magnetizing harmonic currents and DC bus charging current present at the primary side (i_{p1}) are shown in Fig.22(a). Notice that magnetizing current harmonics are significant in this case since a larger portion of the core is being magnetized through a CPAT with 2nd, 3rd and 5th order harmonics at a magnitude of 4.6%, 51.3% and 15.67% respectively. The shunt converter was enabled to supply these harmonic components while maintaining a constant DC Bus as shown in Fig.23(a) and Fig.23(b). The resulting primary current waveform shown in Fig.22(b) illustrates

the effectiveness of the shunt winding to eliminate harmonic components present in the primary current to less than 0.33% of the fundamental component.

Primary reactive power control can be observed in Fig.24 as the reference reactive power is changed from 0VAR such that v_{p1} and i_{p1} are in phase as shown in Fig.24(a) to 2500VAR as shown in Fig.24(b). In this operation scenario, the shunt converter absorbs active power to maintain a constant DC bus while supplying/absorbing reactive power to achieve the required reference reactive power at the primary winding.

A 12kW resistive load was connected to the primary winding to illustrate the possibility of sharing the load power between primary and secondary winding. Power flow control between primary and secondary was achieved by changing the reference power at the secondary (P_{p4}) from -0.5kW to 8.5kW as presented in Fig.25 such that the primary line would supply the remaining 3.5kW of the load. Meanwhile, reactive power at the secondary side (Q_{p4}) was maintained zero.

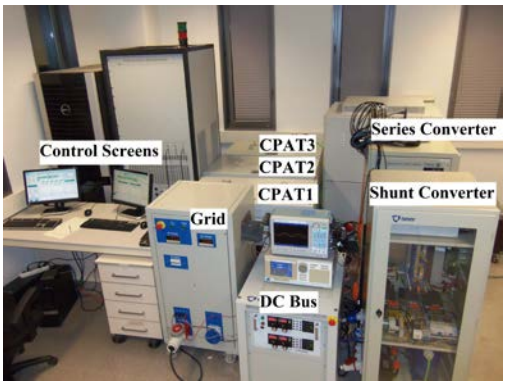

Fig.24. Laboratory setup of three-phase CPAT.

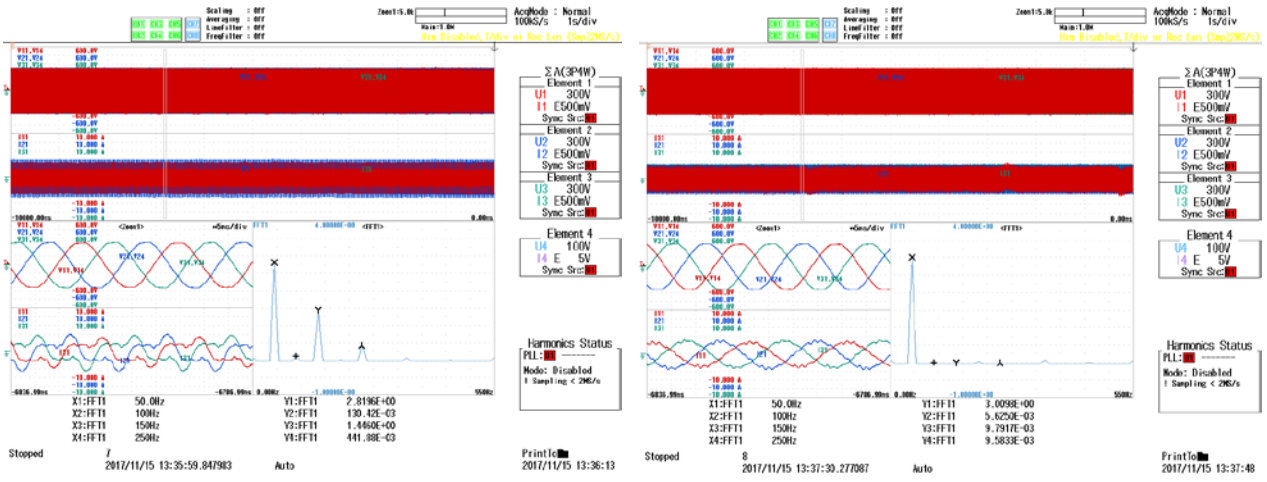

(a) (b)

Fig.25. Primary voltage and current (1sec/div and zoom 5msec/div) (a) without harmonics compensation and (b) with harmonics compensation.

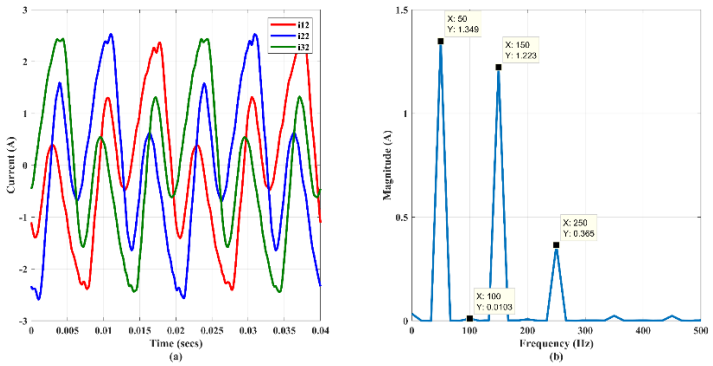

Fig.26. Shunt converter current with harmonics compensation enabled. (a) waveform and (b) harmonics spectrum.

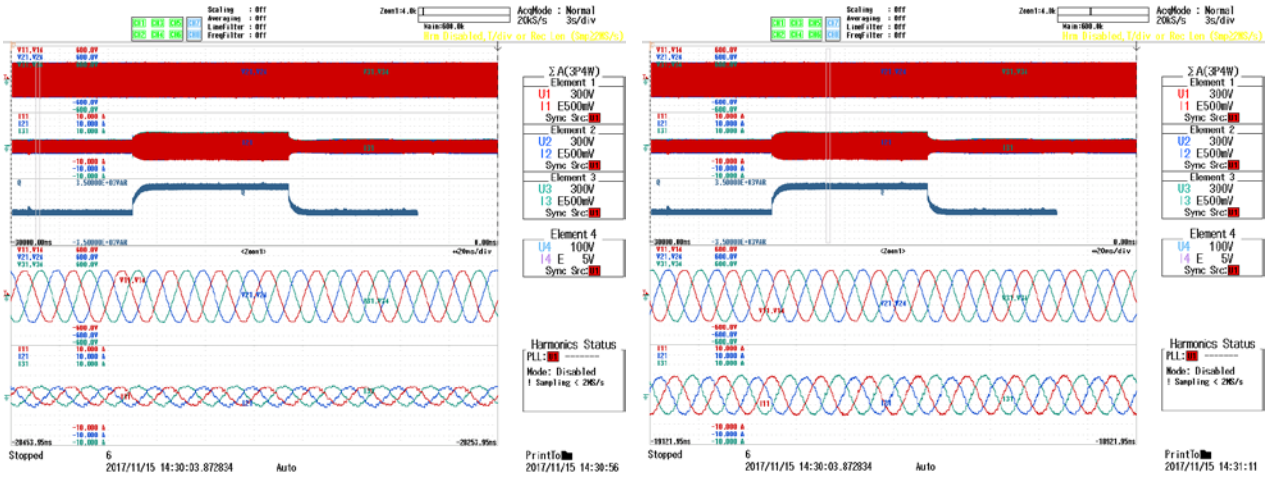

(a) (b)

Fig.27. Primary current reactive power control (3sec/div and zoom 20msec/div) (a) zero reference and (b) 2500VAR reference.

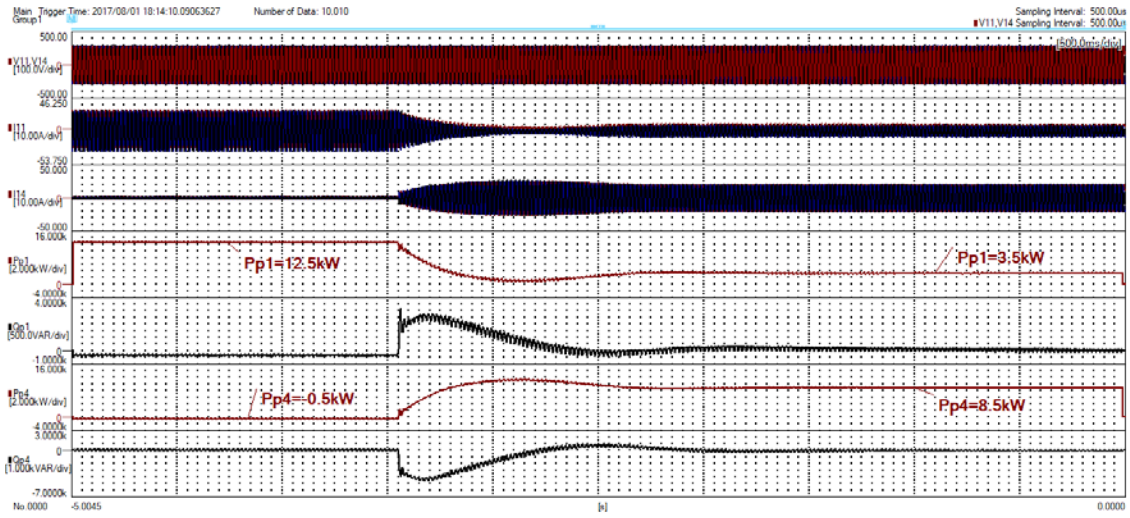

Fig. 28. Transformer power during active power change from -500W to 8.5kW (500msec/div).

B. 5-BUS POWER SYSTEM

To investigate the operation of a three-phase CPAT in a power system, the CPAT was utilized in a 5-bus power system case study shown in Fig.29. The case study consists of two machines G1 and G2 each rated 1000MVA and 1200MVA, respectively. The CPAT was placed between the generator bus (B1) and the transmission bus (B3) to replace a 1000MVA step-up transformer for the 50km transmission line to the load bus (B5). The CPAT was modeled based on the configuration shown in Fig.7 (neglecting hysteresis effect) with the equivalent parameters presented in Table III.

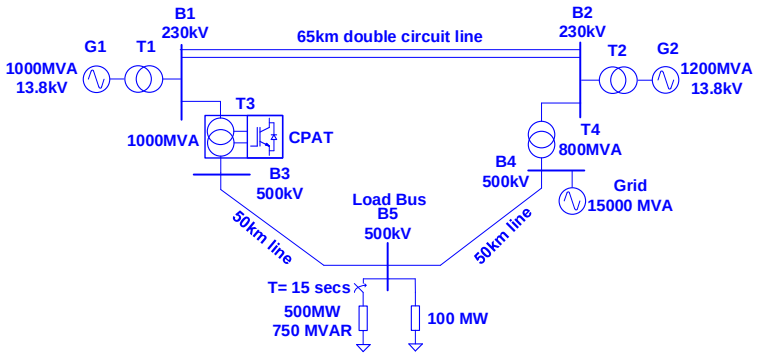

Fig. 29. Single-line diagram of 5-bus power system case study with a three-phase CPAT model.

TABLE II

Parameters of the Average CPAT and Converter Model

Parameter	Value
Simulation step-time	0.1µsec

Rated Power/CPAT	333MVA
v_{p1}, v_{p2}, $v_{p3,}$ v_{p4}	138.5kV, 138.5kV, 138.5kV,288.6kV
R_{pk}, R_{epm}	0.002 p.u., 500 p.u.
$L_{pk,}$ L_{epm}, L_0	0.002 p.u., 500 p.u., 0.003 p.u.
v_{dc1}, v_{dc2}	250kV
Control sampling frequency	10kHz

In this system, the series winding of the CPAT-UPFC is utilized to control active power through the 50km transmission line and regulate the load bus voltage (V_{load}). Since the CPAT-UPFC is not connected at the load bus, a 100msec delay is considered in the measured load bus voltage to account for communication delay [27]. The CPAT also regulates reactive power absorbed between B1 and B3 through its shunt winding. A 500MW,750MVAR load is suddenly connected on bus B5 at T=15secs to investigate the effectiveness of a CPAT to regulate load bus voltage and power flow through the system.

Using the OPAL-RT, a real-time smulation of the 5-bus power system was performed to investigate the stability of the power system with the CPAT in operation. The effect of the CPAT on G1,G2 and the grid during the connection of the 500MW,750MVAR shown in Fig.30. Reduction in G1 active and reactive power oscillations as well as G2 reactive power can be observed with the operation of the CPAT. Moreover, Fig.31 shows the primary and secondary windings oscillations were reduced as the CPAT controllers were enabled.

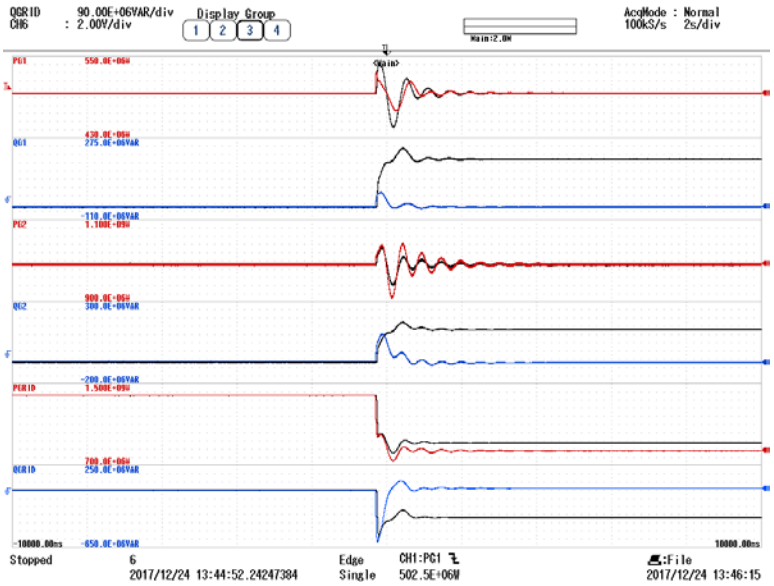

Fig.30. Active and reactive power through G1,G2 and grid without a CPAT (black lines) and with a CPAT.

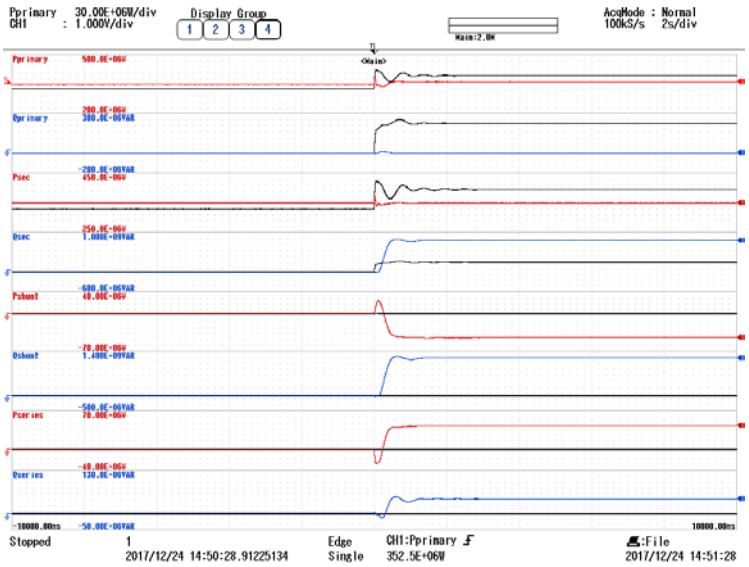

Fig.31. Active and reactive power through transformer windings without a CPAT (black lines) and with a CPAT.

VI. Conclusion

This paper presented the three-phase CPAT in two possible configurations. Both configurations were modeled and analyzed based on their equivalent magnetic circuit showing that both configurations operate identically. Moreover, core structure of the three-phase shell type transformer has been compared to several shunt-series compensation configurations to investigate the limitations and benefits of a three-phase CPAT. The analysis shows that the three-phase CPAT can be mostly beneficial when utilized instead of a compensation system consisting of multiple three-phase transformers. In addition, the CPAT requires a reduced number of windings as well as supporting structure and protection equipment. Finally, simulation and experimental analysis of a power flow control application shows the applicability of a three-phase CPAT to effectively achieve shunt and series services to the grid through fractional power converters.

References

[1] M. Sahraei-Ardakani and S. A. Blumsack, “Transfer Capability Improvement Through Market-Based Operation of Series FACTS Devices,” *IEEE Trans. Power Syst.*, vol. 31, no. 5, pp. 3702-3714, Sept. 2016.

[2] W. Litzenberger, K. Mitsch and M. Bhuiyan, “When It's Time to Upgrade: HVdc and FACTS Renovation in the Western Power System,” *IEEE Power Energy Mag.*, vol. 14, no. 2, pp. 32-41, Mar. 2016.

[3] S. Yang, Y. Liu, X. Wang, D. Gunasekaran, U. Karki and F. Z. Peng, “Modulation and Control of Transformerless UPFC,” *IEEE Trans. Power Electron.*, vol. 31, no. 2, pp. 1050-1063, Feb. 2016.

[4] L. Gyugyi, C. D. Schauder, S. L. Williams, T. R. Rietman, D. R. Torgerson and A. Edris, "The unified power flow controller: a new approach to power transmission control," *IEEE Trans. Power Del.*, vol. 10, no. 2, pp. 1085-1097, Apr. 1995.

[5] C. D. Schauder, L. Gyugyi, M. R. Lund, D. M. Hamai, T. R. Rietman, D. R. Torgerson and A. Edris, "Operation of the unified power flow controller (UPFC) under practical constraints," *IEEE Trans. Power Del.*, vol. 13, no. 2, pp. 630-639, Apr. 1998.

[6] K. Sano and M. Takasaki, "A Transformerless D-STATCOM Based on a Multivoltage Cascade Converter Requiring No DC Sources," *IEEE Trans. Power Electron.*, vol. 27, no. 6, pp. 2783-2795, June 2012.

[7] F. Z. Peng, Y. Liu, S. Yang, S. Zhang, D. Gunasekaran and U. Karki, "Transformer-Less Unified Power-Flow Controller Using the Cascade Multilevel Inverter," *IEEE Trans. Power Electron.*, vol. 31, no. 8, pp. 5461-5472, Aug. 2016.

[8] L. Ferreira Costa, G. De Carne, G. Buticchi and M. Liserre, "The Smart Transformer: A solid-state transformer tailored to provide ancillary services to the distribution grid," *IEEE Power Electron. Mag.*, vol. 4, no. 2, pp. 56-67, Jun. 2017.

[9] Dan Wang, Jie Tian, Chengxiong Mao, Jiming Lu, Yuping Duan, Jun Qiu and Huihong Cai, "A 10-kV/400-V 500-kVA Electronic Power Transformer," *IEEE Trans. Ind. Electron.*, vol. 63, no. 11, pp. 6653-6663, Nov. 2016.

[10] T. L. Vandoorn, J. D. M. De Kooning, B. Meersman, J. M. Guerrero and L. Vandevelde, "Voltage-Based Control of a Smart Transformer in a Microgrid," *IEEE Trans. Ind. Electron.*, vol. 60, no. 4, pp. 1291-1305, Apr. 2013.

[11] Y. Liu, S. Yang, X. Wang, D. Gunasekaran, U. Karki and F. Z. Peng, "Application of Transformer-Less UPFC for Interconnecting Two Synchronous AC Grids With Large Phase Difference," *IEEE Trans. Power Electron.*, vol. 31, no. 9, pp. 6092-6103, Sept. 2016.

[12] P. Li, Y. Wang, C. Feng and J. Lin, "Application of MMC-UPFC in the 500 kV power grid of Suzhou," *The Journal of Engineering*, vol. 2017, no. 13, pp. 2514-2518, 2017.

[13] M. Andresen, K. Ma, G. De Carne, G. Buticchi, F. Blaabjerg and M. Liserre, "Thermal Stress Analysis of Medium-Voltage Converters for Smart Transformers," *IEEE Trans. Power Electron.*, vol. 32, no. 6, pp. 4753-4765, Jun. 2017.

[14] C. Wang, X. Yin, Z. Zhang and M. Wen, “A Novel Compensation Technology of Static Synchronous Compensator Integrated With Distribution Transformer,” *IEEE Trans. Power Del.*, vol. 28, no. 2, pp. 1032-1039, Apr. 2013.

[15] B. B. Ambati and V. Khadkikar, “Variable Frequency Transformer Configuration for Decoupled Active-Reactive Powers Transfer Control,” *IEEE Trans. on Energy Convers.*, vol. 31, no. 3, pp. 906-914, Sept. 2016.

[16] A. Dimitrovski, Z. Li and B. Ozpineci, “Magnetic Amplifier-Based Power-Flow Controller,” *IEEE Trans. Power Del.*, vol. 30, no. 4, pp. 1708-1714, Aug. 2015.

[17] K. K. Sen and Mey Ling Sen, “Introducing the family of "Sen" transformers: a set of power flow controlling transformers,” *IEEE Trans. Power Del.*, vol. 18, no. 1, pp. 149-157, Jan. 2003.

[18] K. K. Sen and Mey Ling Sen, “Comparison of the "Sen" transformer with the unified power flow controller,” *IEEE Trans. Power Del.*, vol. 18, no. 4, pp. 1523-1533, Oct. 2003.

[19] J. Yuan, L. Chen and B. Chen, “The improved Sen transformer — A new effective approach to power transmission control,” *Energy Conversion Congress and Exposition*, Pittsburgh, PA, 2014, pp. 724-729.

[20] M. A. Elsaharty, J. I. Candela and P. Rodriguez, “Custom Power Active Transformer for Flexible Operation of Power Systems,” *IEEE Trans. Power Electron.*, vol. 33, no. 7, pp. 5773-5783, July 2018.

[21] M.A. Elsaharty, Jose Ignacio Candela and Pedro Rodriguez, “Power System Compensation Using a Power Electronics Integrated Transformer”, *IEEE Trans. Power Del.*, vol. PP, no.99, pp.1-1, Sept. 2017.

[22] A. K. R. K. and S. P. Singh, “Congestion mitigation using UPFC,” *IET Generation, Transmission & Distribution*, vol. 10, no. 10, pp. 2433-2442, Jul. 2016.

[23] Yim-Shu Lee, Leung-Pong Wong and D. K. W. Cheng, “Simulation and design of integrated magnetics for power converters,” *IEEE Trans. Magn.*, vol. 39, no. 2, pp. 1008-1018, Mar. 2003.

[24] Y. Lu, G. Xiao, X. Wang, F. Blaabjerg and D. Lu, “Control Strategy for Single-Phase Transformerless Three-Leg Unified Power Quality Conditioner Based on Space Vector Modulation,” *IEEE Trans. Power Electron.*, vol. 31, no. 4, pp. 2840-2849, Apr. 2016.

[25] S. Jazebi et al., “Duality Derived Transformer Models for Low-Frequency Electromagnetic Transients—Part I: Topological Models,” *IEEE Trans. Power Del.*, vol. 31, no. 5, pp. 2410-2419, Oct. 2016.

[26] R. Teodorescu, M. Liserre, and P. Rodriguez, Grid Converters for Photovoltaic and Wind Power Systems. Hoboken, NJ, USA: Wiley, 2011.

[27] E. Rakhshani and P. Rodriguez, “Inertia Emulation in AC/DC Interconnected Power Systems Using Derivative Technique Considering Frequency Measurement Effects,” *IEEE Trans. Power Syst.*, vol. 32, no. 5, pp. 3338-3351, Sept. 2017.